ADVANCED FUNCTIONAL MATERIALS
www.afm-journal.de

Tension Pistons: Amplifying Piston Force Using Fluid-Induced Tension in Flexible Materials

Shuguang Li, Daniel M. Vogt, Nicholas W. Bartlett, Daniela Rus,* and Robert J. Wood**

Pistons are ubiquitous devices used for fluid-mechanical energy conversion. However, despite this ubiquity and centuries of development, the forces and motions produced by conventional rigid pistons are limited by their design. The use of flexible materials and structures opens a door to the design of a piston with unconventional features. In this study, an architecture for pistons that utilizes a combination of flexible membrane materials and compressible rigid structures is proposed. In contrast to conventional pistons, the fluid-pressure-induced tension forces in the flexible membrane play a primary role in the system, rather than compressive forces on the internal surfaces of the piston. The compressive skeletal structures offer the opportunity for the production of tunable forces and motions in the "tension piston" system. The experimental results indicate that the tension piston concept is able to produce substantially greater force (more than three times), higher power, and higher energy efficiency (more than 40% improvement at low pressures) compared to a conventional piston, and these features enable myriad potential applications for the tension piston as a drop-in replacement for existing pistons.

1. Introduction

Numerous machines and devices have been developed to harness power from fluids for agricultural and industrial production throughout human history. The piston is one of the most important inventions in engineering over the past several centuries. It is a simple device that converts fluidic pressure to force and displacement to perform work. It has been widely used in various applications that require very high forces or in transmissions, such as the piston engines and hydraulic (or pneumatic) actuators.

Dr. S. Li, D. M. Vogt, Dr. N. W. Bartlett, Prof. R. J. Wood
John A. Paulson School of Engineering and Applied Sciences
Harvard University
Cambridge, MA 02138, USA
E-mail: lisg@seas.harvard.edu; rjwood@seas.harvard.edu
Dr. S. Li, D. M. Vogt, Dr. N. W. Bartlett, Prof. R. J. Wood
Wyss Institute for Biologically Inspired Engineering
Harvard University
Cambridge, MA 02138, USA
Dr. S. Li, Prof. D. Rus
Computer Science and Artificial Intelligence Laboratory
Massachusetts Institute of Technology
Cambridge, MA 02139, USA
E-mail: rus@csail.mit.edu
The ORCID identification number(s) for the author(s) of this article can be found under https://doi.org/10.1002/adfm.201901419.

DOI: 10.1002/adfm.201901419

A conventional piston is made of hard materials and it is usually tightly contained in a rigid chamber (e.g., a cylinder, as shown in **Figure 1**a). A sealing device or material is used at the interface between the piston and the chamber wall, thus the chamber is separated into two isolated spaces by the piston head. These two spaces are connected to different fluid sources (or an ambient fluid, such as air) through fluid ports. If the fluids in these two spaces have different pressures, then the piston will be driven to slide or rotate along and inside of the chamber wall by a compressive force due to this pressure difference. The amplitude of this pressure-induced force, F, is in a linear relationship with the cross-sectional area of the piston head, A, and the pressure difference ΔP as $F = \Delta P \times A$. A rigid rod or a flexible cable is attached to the piston; thus, this sliding or rotating motion can be transmitted outside of the chamber. However, conventional piston systems can face serious problems of friction and leakage due to the tight contacts and sliding motions between the piston and the chamber walls.

Flexible materials have been introduced into the classic piston design to overcome these friction and leakage issues. A rolling diaphragm can be used to connect and seal the piston and the chamber wall, and this kind of fluid-tight diaphragm is both flexible and strong. Thus, the rolling diaphragm piston can have negligible friction, zero-leakage, and very low hysteresis.[1–5] Furthermore, a fluid-driven actuator can be created without an internal "piston" and the chamber can be made of flexible materials, such as air springs and bellow-shaped actuators.[6–8] These flexible-wall actuators can generate axial expanding or contracting motions if the chamber's internal fluid pressure differs from the external pressure. Similar to the rolling diaphragm piston, the friction and leakage of this kind of actuation can be negligible. However, both of these flexible-material-based actuators have relatively short strokes, and their output forces are limited by the area of the rigid ends A, as with conventional pistons.

Flexible membrane materials have also been used in fluid-pressure-driven actuators to produce tension forces for contractile motions.[9–12] These tension forces, T, can be significantly greater than the pressure-induced longitudinal compressive forces ($F = \Delta P \times A$) on the actuators' rigid ends. For example, McKibben-type soft actuators can be driven by pressurized fluids (<500 kPa) to produce blocked actuation stresses of more

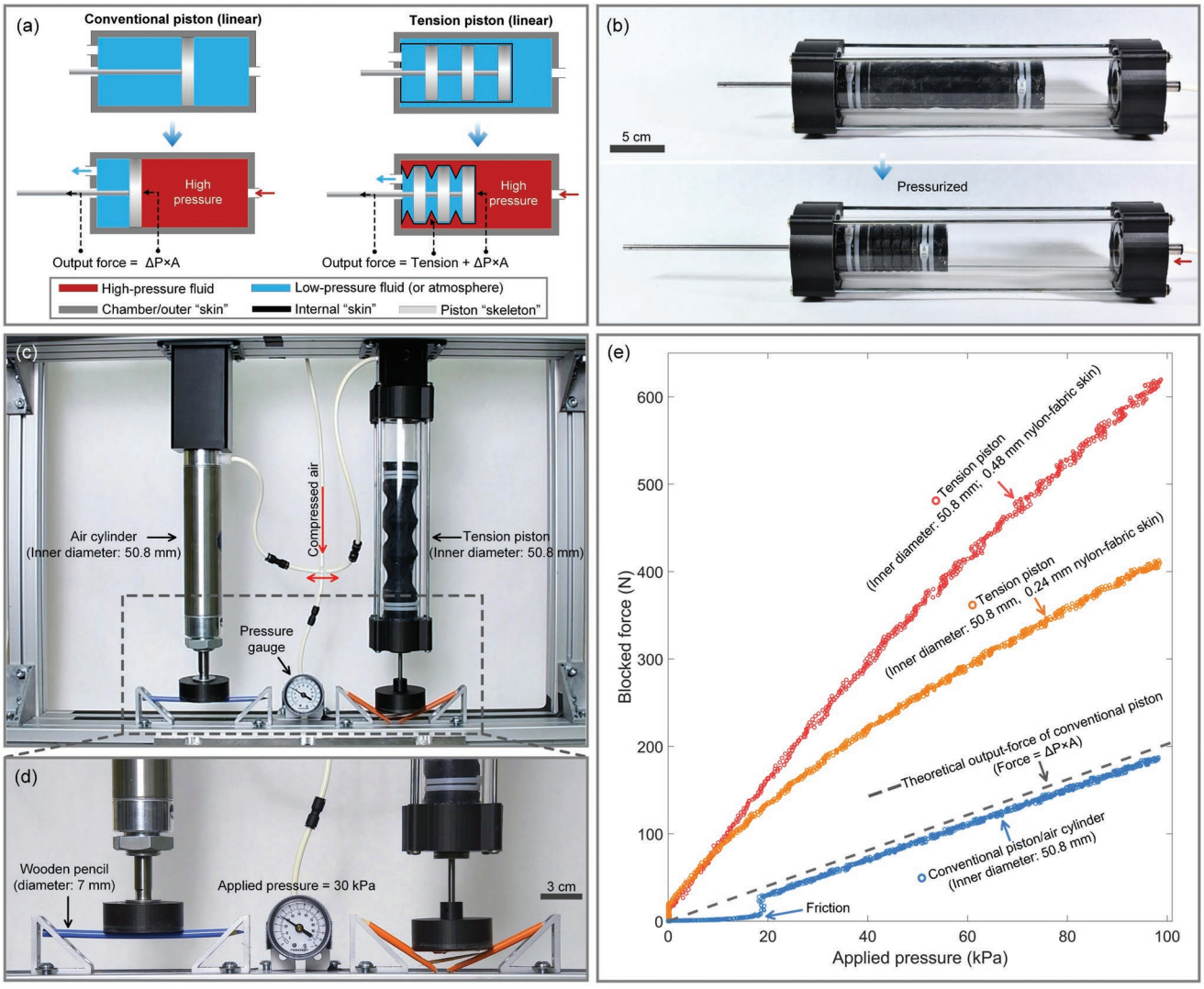

Figure 1. a) Working principles for a conventional piston (left) and a tension piston (right). b) A prototype of the linear tension piston. c,d) An object-crushing comparison between a conventional piston (air cylinder) and a tension piston at the same driving air-pressure. e) A comparison of the output forces of a conventional piston (air cylinder) and two tension pistons with different skin materials.

than 1 MPa,[12,13] however, their contraction ratios are usually small (≈30%) and the actuators become bulky in the radial direction once pressurized. Morin-type actuators can produce axial forces based on the fluid-pressure-induced tensions in their flexible membranes without volumetric expansion, but their strokes are often limited by their slender diaphragm design.[12,14,15] Vacuum-driven soft actuators[16–20] can produce large contractile strokes (up to 90%) with relatively compact shapes, however, the tension force for actuation is limited by the maximum vacuum pressure level (≈−100 kPa).

Here we propose a new architecture, named the "tension piston" that can convert fluid pressure to mechanical force and vice versa. The tension piston uses fluid-pressure-induced tension forces in a flexible membrane to drive a compressible rigid skeletal structure for force and motion transmission (Figure 1b). This tension-driven piston can be used to produce both translational and rotational actuation with large output force (or torque) and substantial stroke (or rotation).

2. Working Principle and Prototypes

As shown in Figure 1a, a basic tension piston consists of six fundamental components: a fluid-tight chamber, a flexible and fluid-tight piston skin, a compressible piston skeleton, an output connector, a higher-pressure fluid medium, and a lower-pressure fluid medium. In this system, the chamber houses the components and separates the fluids. The piston skin separates the inside-piston fluid and inside-chamber (outside-piston) fluid by covering and sealing the piston skeleton inside the chamber. It is made of a thin material that is sufficiently flexible to allow compression, and strong enough to transfer the tension force. The piston skin needs to be fixed on the chamber and skeleton to enable an efficient tension-force generation. The piston skeleton is a compressible solid structure with multiple voids, and these voids allow the skeleton to be compressed to produce the desired transformation by the piston skin under a fluidic pressure difference. The output connector is fixed on the piston's

skeleton, and it can transmit the skeleton's motion and force (or torque) to the outside of the chamber. A fluidic pressure difference is necessary to produce tensional and compressive forces on the piston skin and skeleton, respectively. This pressure difference can be generated by either pressurizing the inside-chamber fluid or depressurizing the inside-piston fluid.

In contrast to conventional pistons, the tension piston's skeleton is driven to contract to produce the desired motion, and this transformation relies on not only the compressive force acting on the skeleton's rigid parts (e.g., force at the end segment $F = \Delta P \times A$), but also the fluid-pressure-induced tension force T on the piston skin as $F = T + \Delta P \times A$ (as shown in Figure 1a and Figure S16, Supporting Information). Therefore, the output force of a tension piston can be much greater than the force produced by a conventional piston with the same inner diameter at the same driving pressure.

To validate the design and performance of the tension piston architecture, we fabricated a set of linear tension pistons using different materials (see **Figure 2** and Supporting Information). A comparison of the working principles between a conventional piston and the tension piston can be found in Movie S1 and Figure S1 of the Supporting Information. The linear tension piston shown in Figure 1b is made of an acrylic cylindrical-shaped chamber (inner diameter: 50.8 mm), a thin air-tight nylon fabric skin (thickness: 0.24 mm), and a plastic skeleton structure with several discrete discs arranged in parallel and sliding along a steel rod. This piston can produce a pushing force and an extension motion on the steel rod when the air inside the chamber is pressurized. The force and motion will terminate when the piston skin and skeleton are compressed into a minimally contracted configuration.

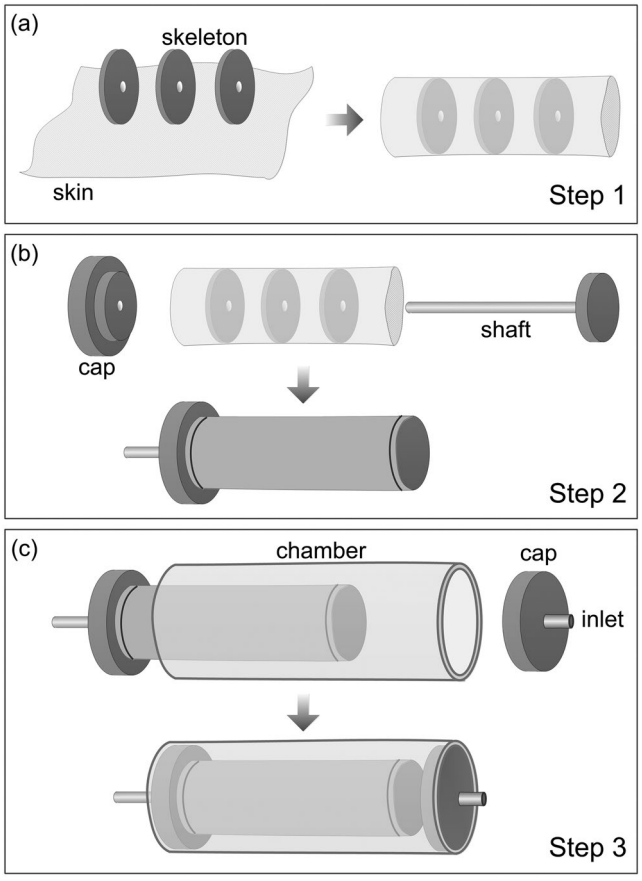

Figure 2. Fabrication process for the linear tension piston. a) Step 1: bonding the skin to the skeleton. b) Step 2: assembling the shaft, skeleton, and skin. c) Step 3: assembling the piston, cylinder/chamber, and caps.

We conducted an object-crushing test to compare the output forces between conventional and tension pistons with the same diameter (50.8 mm). A metal framework was built to hold the two different pistons vertically and the direction of the output force and rod extend are both toward the ground. In each test, a pair of identical test objects were placed above the bottom metal frame and under the press heads of the piston rods. Compressed air was used to power these two pistons through a cross-shaped tubing connection, and a pressure gauge was used to indicate the applied pressure. This tubing connection can supply pressurized air to each piston and the pressure gauge at the same pressure level. A group of objects including raw eggs, wooden pencils, and plastic bottles were tested (see Supporting Information), and it was observed that the tension piston always broke the same object at a lower pressure compared to the conventional piston (air cylinder, BIMBA 314-XP). In an example shown in Figure 1c,d, the tension piston breaks a wooden pencil (diameter: 7 mm) at 30 kPa pressure while the conventional air cylinder cannot damage a similar pencil. These qualitative results indicate that the tension piston can produce greater force than the conventional piston at the same applied pressure (see Movie S2, Supporting Information).

Furthermore, we performed a complete static force test on a conventional piston (air cylinder) and two tension pistons with different skin materials (0.24 and 0.48 mm nylon fabric membranes). Figure 1e shows the comparison of the experimental static (blocked) forces from these three pistons over three trials at different air pressures, as well as the theoretical force outputs based on the relationship $F = \Delta P \times A$. As shown in the figure, the blocked force increases as the applied air pressure increases for all three pistons. The air cylinder's force fits well with the theoretical model of the conventional piston, however, a significant stiction behavior appeared in the low-pressure region (<20 kPa). By contrast, the two tension pistons seem very sensitive to small pressure changes, and they started to produce forces at extremely low pressures without stiction. Most importantly, both of the tension pistons produced significantly greater forces than the air cylinder at the same levels of applied pressure. Compared to the air cylinder's force outputs, the tension piston with 0.24 mm nylon fabric skin can generate two times greater forces. More interestingly, the tension piston using a thicker skin material (0.48 mm thickness) can produce more than three times greater force. These results indicate that the stronger and less-stretchable skin material might be more efficient for tension force production and transmission processes in our piston system.

3. Configurations and Materials for the Tension Piston

The tension piston can be constructed with a wide variety of configurations and materials. The skeleton can be built

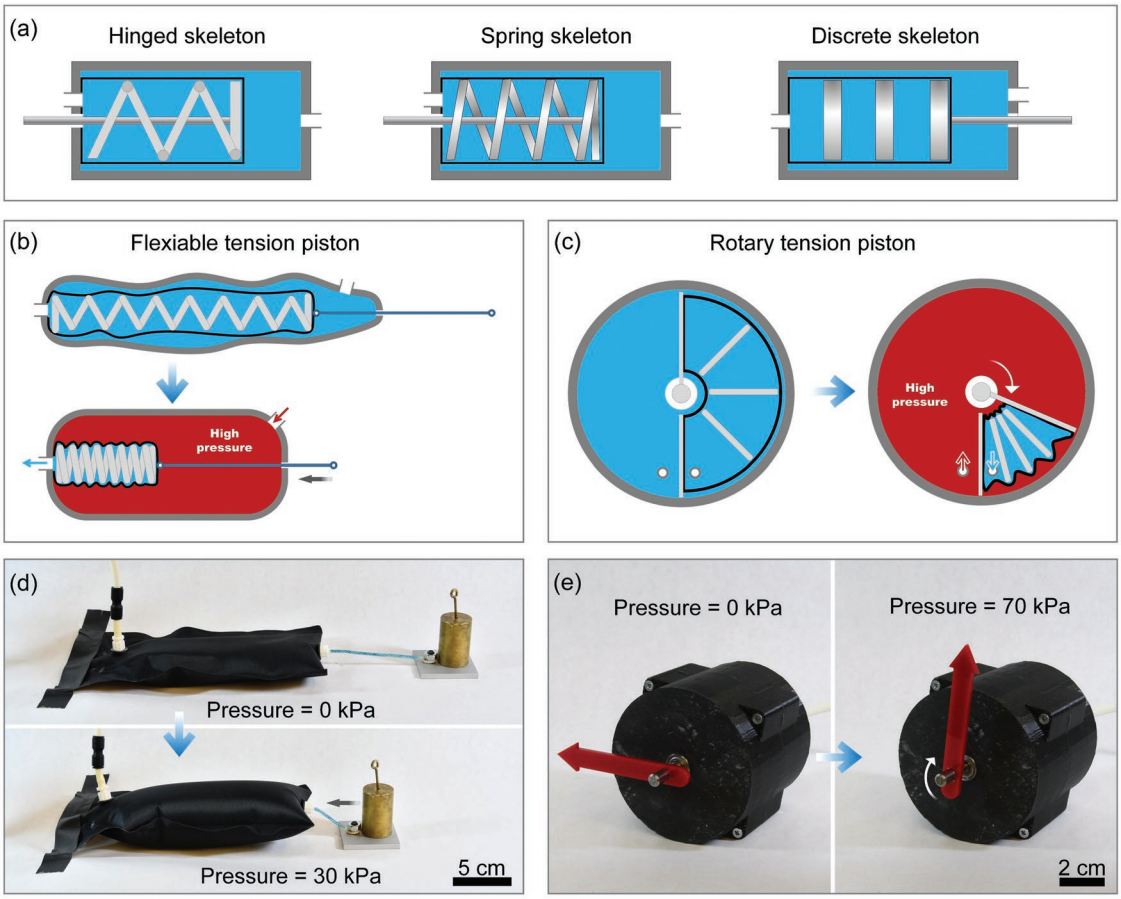

Figure 3. a) Different skeletal configurations for linear tension pistons. b) The design and d) a prototype of a tension piston with a flexible outer chamber. c) The design and e) a prototype of a tension piston with rotary motion.

from one piece of compressible material or structure and, alternatively, it can be assembled from discrete elements in either a jointed configuration or a separated configuration (**Figure 3**a). Springs and elastic materials can be used to join those elements together.[21,22] The structural voids can be arranged into different geometrical patterns, and the skeleton elements can also be constructed from different materials. These features allow the piston skeleton to produce motions with tunable amplitudes in multiple directions, and even at different rates.

Similarly, the piston chamber can be made of either rigid or flexible materials (Figure 3b,d; Movie S3, Supporting Information), however, it should have sufficient strength to contain other components under expected operating fluid pressures. It can take on any 3D geometry that allows the internal components (e.g., piston skeleton) to move, such as a cylindrical or prismatic chambers for translational piston motions or a cylindrical or spherical chambers for rotational piston motions (Figure 3c,e; Movie S3, Supporting Information). It should be noted that multiple tension pistons can be installed inside a single chamber to produce complex multiple-axial motions using a single fluid pressure source.

The output connector can be a rigid rod or even a flexible cable. It can be attached to a particular location on the piston skeleton either inside or outside of the piston skin to transmit desired output motions, for example, pushing or pulling motions (Figure S2, Supporting Information). It is also possible to attach multiple rods or cables to a single piston skeleton for multidirectional outputs.

The ideal materials for the tension piston's skin should be flexible and non-stretchable. These materials should also be resistant to both the fluids inside and outside of the piston. For a single-acting piston motion, using springs and elastic materials can help the skeleton to return to its original shape after actuation, and the piston skin need not be bonded on the piston skeleton. However, the piston skin must be bonded onto the skeleton in order to achieve a double-acting piston motion. In this case, the inside-piston fluid can be pressurized to drive the piston to return to its original shape.

The fluid medium inside of the piston (or inside of the chamber) can be directly connected to ambient pressure through a port, or it can also be connected to a separate fluid source. The inside-piston fluid can be the same as the inside-chamber fluid, or it can alternatively be a different kind of fluid. Other methods, for example heating and cooling, might also be used to pressurize or depressurize the fluids, if the fluids are completely contained inside the chamber and piston, without connection to the external fluid sources.

4. Modeling of the Linear Tension Piston

In this paper, we primarily focus on the basic linear cylindrical tension piston configuration with a skeleton composed of several discrete parallel discs, as shown in the conceptual diagram Figure 1b. Here, we first investigate the interaction between pressure changes, the skin deformation, and the skeleton's geometry in this linear tension piston. In our study, the tension piston's aspect ratio is defined as $R = L/D$, where L is the space between two skeletal disks, and D is the diameter of each disk. We then fabricated four tension pistons with the same disk diameter D of 46 mm (disk thickness = 5 mm; acrylic chamber diameter = 50.8 mm), but varying the spaces between each disk: 16.5, 28, 51, and 74 mm (see Figures S3–S7, Supporting Information). Thus the four pistons have aspect ratios of 0.25, 0.5, 1.0, and 1.5, respectively. A thin nylon fabric sheet (thickness = 0.24 mm) is used as the skin material for these four pistons. **Figure 4**a shows a comparison of the four pistons at 100 kPa air pressure in blocked force tests. Interestingly, we found that all the pistons' skins contract radially, and generate a group of evenly distributed "wrinkle" patterns at each segment. The pistons with larger aspect ratios seem to have less but deeper skin "wrinkles" than smaller-aspect ratio pistons. To quantitatively characterize the skin's deformation under pressure, we also built a single-beam 2D laser scanner (Figure S8, Supporting Information). Using this scanner, we can measure the skin's deformation profile (the winkle's depth along the segment's length) from the outside of the pressurized transparent acrylic chamber.

To further investigate the tension pistons, we also built a numerical model-based finite element method (FEM) using ABAQUS software. The skin material's tensile modulus and Poisson's ratio used in this model were derived from physical tensile tests of the materials used (Figures S9 and S10, Supporting Information). Figure 4b shows simulations of the four pistons' last segments at 100 kPa applied pressure. The simulated skin deformations are in good agreement with the experimental results shown in Figure 4a and Movie S4 (Supporting Information).

Moreover, we compared the laser measurements and the FEM results of the wrinkle depths over one segment of each piston. As the comparison shows in Figure 4c, the FEM simulations (dashed lines) match consistently with the experimental data (solid lines) at different driving air pressures (20 to

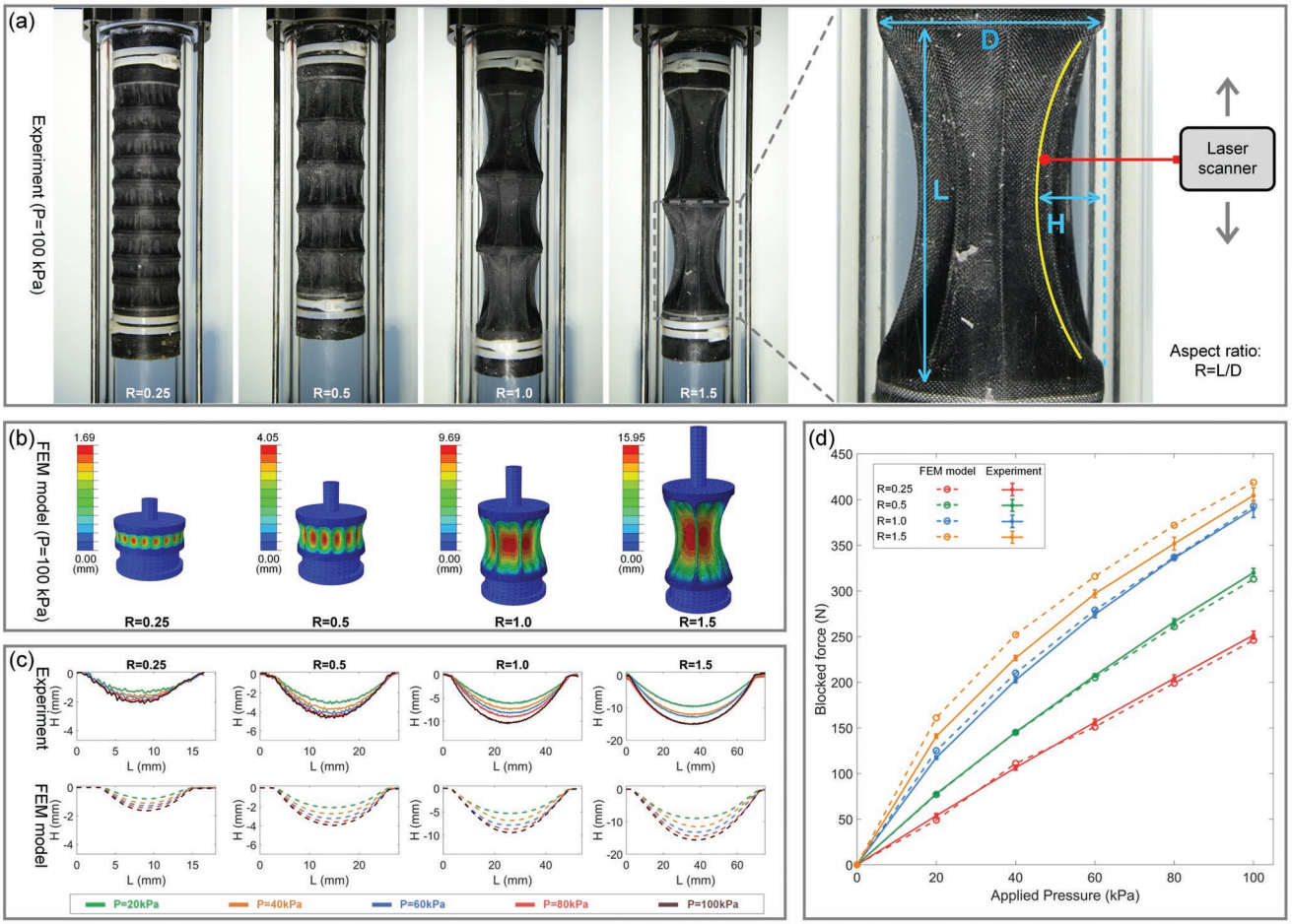

Figure 4. Linear tension piston designs with different aspect ratios. a) Skin deformation comparison experiments. b) Skin deformation comparisons using FEM modeling. c) Comparison of the skin wrinkle profile between laser measurements and FEM model predictions. d) Comparison of the blocked forces between experimental measurements and FEM model predictions.

100 kPa). Both reveal similar parabolic skin deformations, and the depths of the skin wrinkles increase as the pressure increases.

We also used this numerical model to predict the output forces of our tension pistons at different pressures. Figure 4d shows a comparison of the blocked forces between the FEM model prediction simulations (dashed lines) and the experimental measurements (solid lines). As observed in most of the cases, our FEM model can accurately predict the blocked forces with negligible errors. However, for the tension piston with a large aspect ratio ($R = 1.5$), the model predicts ≈15% greater forces than the measured results. This predication error might due to fabrication defects or loose skin-skeleton bonding under large forces.

The experimental results in Figure 4d also reveal that the aspect ratio plays an important role in the performance of force and extension of the linear tension piston. The tension piston with a greater aspect ratio can produce a greater blocked force compared to the tension piston with a smaller aspect ratio at the same pressure. For example, the piston with an aspect-ratio of 1.5 produced a blocked force greater than 400 N at 100 kPa driving pressure, while the piston with an aspect-ratio of 0.25 generated a blocked force of ≈250 N at the same pressure. Thse results indicate that a greater surface area of the skin can produce a greater tension force in the tension piston system.

However, in general the piston with a smaller aspect ratio skeleton has a greater axial extension ratio (the load-free full extension normalized to the original length of the skeleton) than the piston with a greater aspect ratio. We observed an extension ratio of over 0.6 from the 0.25-aspect-ratio tension piston, and an extension ratio of ≈0.35 from the 1.5-aspect-ratio tension piston, both at the same driving pressure of 100 kPa (see Figure S11, Supporting Information). This reduction of extension ratio is mainly due to the increased skin between two skeleton disks, as the skin can be fully folded or crumpled before the skeleton is compressed. Thus the more crumpled skin produces a greater resistance against the complete compression of the skeleton.

In addition, the nonlinearity between the applied pressure and blocked force becomes more significant as the tension piston's aspect ratio increases. This phenomenon may be due to energy loss from skin elongation, and the increased deflection angle between the skin surface (tension direction) and the longitudinal axis (blocked force direction) at the edges of each skeleton disc for pistons with a larger aspect ratio. The variation of the skin deflection angle as a function of the aspect ratio can be seen in Figure 4c.

5. Characterization of Energy Conversion Efficiency

We quantified the fluidic-to-mechanical energy conversion efficiencies for a linear tension piston (aspect ratio = 1.0) and a conventional air cylinder with the same inner diameter (50.8 mm). The energy efficiencies of the two pistons were characterized through two groups of quasi-static loading tests at different driving pressures. The applied pressures in the first group of the tests were started from 0 kPa and were then maintained at the required levels (including the initial pressurization process). By contrast, we pressurized the pistons to the required pressure levels before each test started in the second group (excluding the initial pressurization process). The experimental results on energy efficiency, air pressure, and flow rate of the two pistons from these two groups of tests are shown in **Figure 5**a,b and c,d, respectively.

For the first group of tests (see Figure 5a), the maximum efficiency of the tension piston is ≈55% at 20 kPa driving pressure, while the air cylinder's maximum efficiency is 67% at 80 kPa driving pressure. However, both of their efficiencies drop gradually when the applied pressure increases, and this might be due to the energy losses from thermal dissipation and system leakages when the internal air is highly compressed.

The tension piston (T-P) exhibits higher efficiencies compared to the air cylinder (conventional piston, C-P) at low pressures (<20 kPa) as the results show in Figure 5a. This efficiency advantage might be due to the energy loss from the air cylinder's static friction. However, the efficiencies of the air cylinder become higher than the efficiencies of the tension piston, and this advantage increases from 10% to 33% as the driving pressure increases from 40 to 120 kPa. This substantial reduction of efficiency in the tension piston is likely caused by the increased volume between the chamber and the skin, due to skin elongation during the initial pressurization process.

Figure 5b shows the flow rate and pressure curves from the tests at 100 kPa driving pressure. The tension piston took ≈20 s to raise its internal air pressure to 100 kPa while the same process was finished within 4 s for the air cylinder. The maximum flow-rate in the tension piston's initial-pressurization phase is 4.16×10^{-5} L min^{-1}, which is 51% greater than the maximum flow-rate (2.75×10^{-5} L min^{-1}) in the air cylinder initial pressurization phase. It seems that the tension piston used a substantially greater volume of compressed air than the air cylinder before the force output (loading phase) in the tests. Therefore, the tension piston's energy efficiency becomes lower.

We conducted a second set of tests using a regulated pressure supply at the beginning of each test. As shown in Figure 5c, the energy efficiencies of the tension piston and the air cylinder are both improved in these tests. The air cylinder's efficiency improvements are 3% to 7% at different pressures, and the maximum efficiency is ≈71% at a driving pressure of 80 kPa. More importantly, the tension piston's efficiency is boosted substantially, with an increase of 10% to 50% at different pressures, and the maximum efficiency is over 90% at a driving pressure of 40 kPa. Moreover, the tension piston's efficiency is generally higher than the conventional air cylinder's efficiency with an improvement of 10% (at 120 kPa) to 64% (at 20 kPa), and this advantage decreases as the applied air pressure increases.

Figure 5d shows the flow rate changes in the two pistons during operation. The air cylinder has a constant input flow rate (at 100 kPa), whereas the tension piston has a varying flow rate (internal volume change) during the test. This nonconstant input flow rate can be attributed to the compressible skeleton of the tension piston, which can have a varying volume change during contraction.

These two groups of experimental results indicate that the skin stretchability of the tension piston has a significant impact on its fluidic-mechanical energy conversion efficiency. The stretched skin can induce an additional volume between

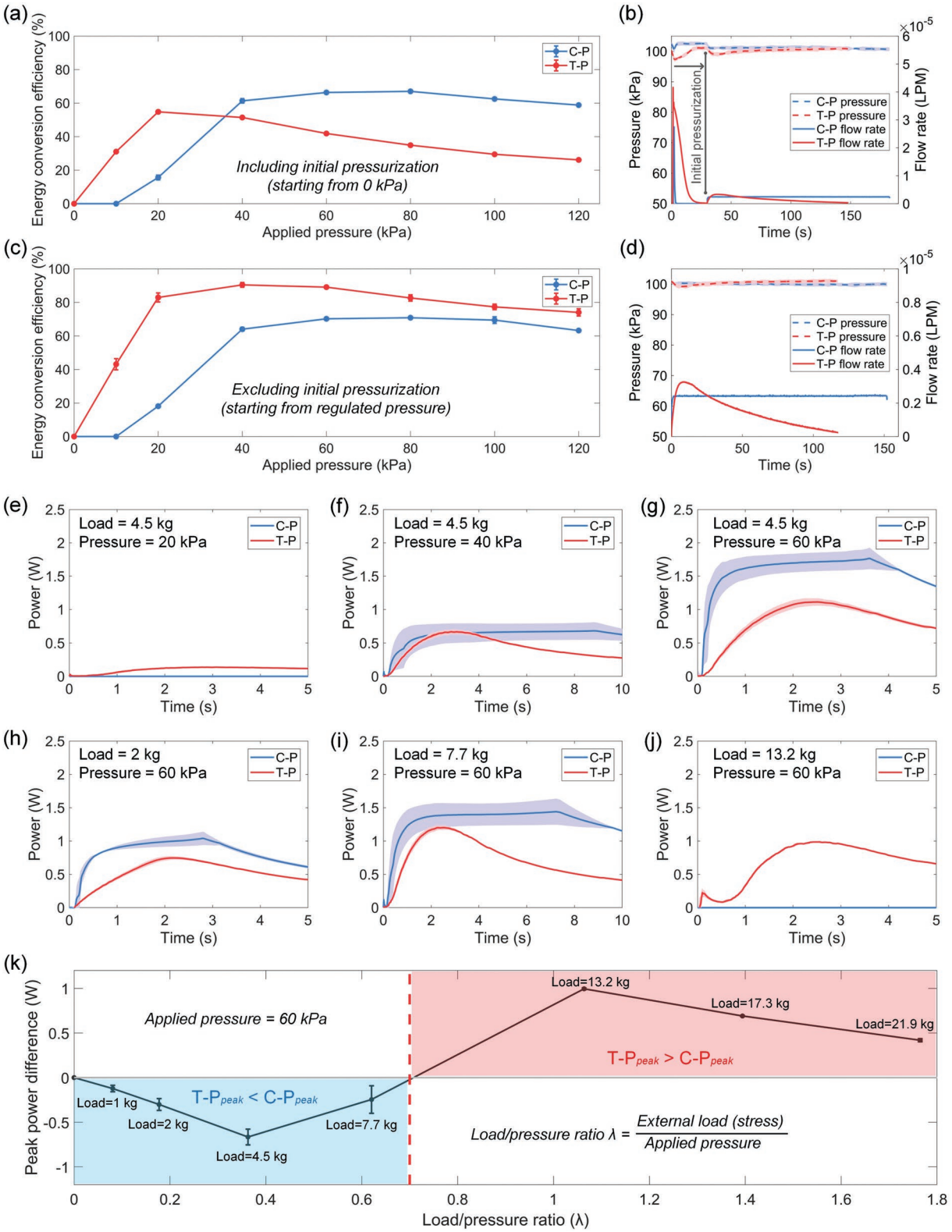

Figure 5. Comparisons of energy conversion efficiency and output power between an air cylinder (C-P) and a linear tension piston (T-P). a) Energy efficiency comparison including the initial pressurization process, and b) the flow rate and pressure comparison at a driving pressure of 100 kPa. c) Energy efficiency comparison excluding the initial pressurization process, and d) the flow rate and pressure comparison at a driving pressure of 100 kPa. e–g) Output power comparison using a fixed load at different air pressures. h–j) Output power comparison using different loads at a fixed air pressure. k) Comparison of the peak power differences at different load/pressure ratios.

the tension piston and its outer chamber under pressure, thus additional compressed air is needed to drive the piston at a constant pressure level. To address this issue and improve the efficiency, low-stretch, high-strength, and flexible membranes or composites (e.g., straight fiber reinforcement[12,23–25]) can be used in the tension piston's skin. It is also possible to use a spring or accumulator mechanism to maintain the required initial pressure (or force) for the tension piston's skin.

6. Characterization of Output Power

To characterize the output power of the tension piston and the air cylinder, we conducted a series of load-lifting tests on these two pistons using various loads at different air pressures (Figure S12 and Movie S5, Supporting Information). The output power was calculated based on a dynamic measurement of the output work over time in each test, and the details of the calculation, measurement, and comparison can be found in Supporting Information.

Figure 5e–g presents output power comparisons between the tension piston and the air cylinder from one of the tests using the same external load (4.5 kg weight) at different driving pressures (20a, 40, and 60 kPa). These results reveal that the peak power increases as the applied pressure increases for a given load in both of the pistons. The air cylinder's peak power increases more than the tension piston's peak power for the same pressure increment, however, the tension piston shows a higher peak power than the air cylinder at low pressures (e.g., ≈ 0.14 W at 20 kPa in Figure 5e).

We also compared the power between the two pistons at the same driving pressure but with various loads. Figure 5h–j shows the experimental results from one of the tests using different loads (2, 7.7, 13.2 kg) at a fixed air pressure of 60 kPa. We found that the output peak power in both pistons increases as the load increases until a certain threshold, and it drops when the load further increases. Most importantly, the result in Figure 5j indicates that the tension piston can still generate a high power (≈1 W) even when the external load becomes larger (13.2 kg) than the air cylinder's maximum lifting capacity (≈12.4 kg at 60 kPa).

Moreover, we introduce a new parameter λ, as the load/pressure ratio, to fully characterize the output power behavior of the two pistons. The load/pressure ratio is defined as the normalized external load (or stress) over the applied pressure in the piston. Figure 5k presents the peak power difference between the two pistons at different values of λ, when the applied pressure is fixed at 60 kPa. The result shows that the air cylinder outputs a higher peak power than the tension piston when λ is smaller than 0.7. However, the tension piston's peak power becomes higher than the air cylinder's peak power if λ is greater than 0.7, and this advantage still remains up to a value of 2.0 in this group of tests. It should be noted that $\lambda = 1.0$ corresponds to the theoretical maximum load-lifting capacity of a conventional piston at a given pressure. This comparison reveals that the tension piston is able to produce a higher peak power than the conventional piston with a large external load at a low driving pressure. It should be noted that the tension pistons used this study have not been optimized for power output and energy efficiency.

7. Conclusion

In this paper, we presented a concept for a tension-driven piston. In contrast to conventional pistons with rigid bodies, the tension piston consists of a flexible skin and a compressible skeleton. This flexible-rigid hybrid piston architecture offers several advantages compared to conventional pistons despite several hundred years of development of the latter. For example, the system can be built with a compliant body and with various configurations. The friction between the tension piston and the chamber wall can be negligible. By using the fluid-induced tension force in the skin, the tension piston can produce a greater force compared to a conventional piston at the same driving pressure. The output force and motion can be tuned by using different designs for the compressible skeleton. We also demonstrated that the tension piston can outperform conventional pistons with substantially higher power and energy efficiency. Therefore, the tension piston has a very broad field of potential applications. It can be used as a device to convert fluid pressure (or energy) to force (or torque) and motion, such as a valve, an actuator, or an engine (see Movie S6, Supporting Information), etc. Alternatively, it can also be used as a device, such as a pump, a compressor, a shock-absorber (or damper), or an energy storage device, etc., to convert force (or torque) to fluidic pressure (or energy). However, there are some weaknesses that limit the practical engineering uses of the current tension pistons. For example, the current tension piston prototypes can only produce single-acting piston motions, thus they cannot be driven reversely by fluid pressure as they are currently designed. More importantly, the skin materials and bonding methods are not ideal for high-strength (pressure) and high-temperature applications. We will address these important issues to expand the utility of the tension pistons in our future work.

8. Experimental Section

In the skin material characterization, a camera was used to record the displacements of the four reference markers during tensile tests, and then an open source image analyzing software (Tracker, http://physlets.org/tracker/) was used to obtain the sample's strains the at axial and transverse directions. In the energy efficiency characterization, an airflow sensor (Honeywell AWM5101) was used to measure the flow rate in the system. In the output power characterization, a video camera was used to record the load's vertical lifting movement driven by the piston. See, Supporting Information for more details.

Supporting Information

Supporting Information is available from the Wiley Online Library or from the author.

Acknowledgements

This paper is based on the work supported by Defense Advanced Research Projects Agency Award (FA8650-15-C-7548), National Science Foundation Awards (IIS-1226075, IIS-1226883, CCF-1138967, NRI-1830291, and EFRI-1830901), and the Wyss Institute for Biologically Inspired Engineering. Any opinions, findings, and conclusions or

recommendations expressed in this material are those of the authors and do not necessarily reflect the views of the National Science Foundation.

Conflict of Interest

The authors declare no conflict of interest.

Keywords

actuators, artificial muscles, flexible materials, pistons, soft robotics

Received: February 15, 2019
Revised: April 12, 2019
Published online:

[1] J. P. Whitney, M. F. Glisson, E. L. Brockmeyer, J. K. Hodgins, presented at *2014 IEEE/RSJ Int. Conf. on Intelligent Robots and Systems*, Chicago, IL, USA, September **2014**.
[2] N. Burkhard, S. Frishman, A. Gruebele, J. P. Whitney, R. Goldman, B. Daniel, M. Cutkosky, presented at *2017 IEEE Int. Conf. on Robotics and Automation*, Singapore, June **2017**.
[3] J. F. Taplin, *US Patent 3250225*, **1966**.
[4] J. V. Smith, *US Patent 3375759*, **1968**.
[5] D. W. Comstock, P. B. Marchetti, *US Patent 3969991*, **1976**.
[6] W. H. Geno, D. A. Weitzenhof, *US Patent 4712776*, **1987**.
[7] X. Yang, Y.-C. Tai, C.-M. Ho, presented at *1997 Int. Conf. on Solid State Sensors and Actuators*, Chicago, IL, USA, June **1997**.
[8] M. Boyvat, D. M. Vogt, R. J. Wood, *Adv. Mater. Technol.* **2018**, *4*, 1800381.
[9] L. Wang, F. Iida, *IEEE Rob. Autom. Mag.* **2015**, *22*, 125.
[10] S. Kim, C. Laschi, B. Trimmer, *Trends Biotechnol.* **2013**, *31*, 287.
[11] D. Rus, M. T. Tolley, *Nature* **2015**, *521*, 467.
[12] F. Daerden, D. Lefeber, *Eur. J. Mech. Environ. Eng.* **2002**, *47*, 11.
[13] C.-P. Chou, B. Hannaford, *IEEE Trans. Rob. Autom.* **1996**, *12*, 90.
[14] M. A. Henri, *US Patent 2642091*, **1953**.
[15] A. Palko, J. Smrcek, *Ind. Rob: Int. J.* **2011**, *38*, 11.
[16] S. Li, D. M. Vogt, D. Rus, R. J. Wood, *Proc. Natl. Acad. Sci. USA* **2017**, *114*, 50.
[17] D. Yang, B. Mosadegh, A. Ainla, B. Lee, F. Khashai, Z. Suo, K. Bertoldi, G. M. Whitesides, *Adv. Mater.* **2015**, *27*, 6323.
[18] D. Yang, M. S. Verma, J. H. So, B. Mosadegh, C. Keplinger, B. Lee, F. Khashai, E. Lossner, Z. Suo, G. M. Whitesides, *Adv. Mater. Technol.* **2016**, *1*, 1600055.
[19] M. A. Robertson, J. Paik, *Sci. Rob.* **2017**, *2*, eaan6357.
[20] W. M. Felt, M. A. Robertson, J. Paik, presented at *2018 IEEE Int. Conf. on Soft Robotics*, Livorno, Italy, April **2018**.
[21] K. Zampaglione, A. P. Sabelhaus, L.-H. Chen, A. M. Agogino, A. K. Agogino, presented at *2016 ASME Int. Design Engineering Technical Conf. and Computers and Information in Engineering Conf.*, Charlotte, NC, USA, August **2016**.
[22] J. Hughes, P. Maiolino, F. Iida, *Sci. Rob.* **2018**, *3*, eaau3098.
[23] Y. Yamada, A. Kojima, Y. Higashi, M. Okui, T. Nakamura, presented at *2018 IEEE Int. Conf. on Biomedical Robotics and Biomechatronics*, Enschede, The Netherlands, August **2018**.
[24] A. Kojima, M. Okui, Y. Yamada, T. Nakamura, presented at *2018 IEEE Int. Conf. on Soft Robotics*, Livorno, Italy, April **2018**.
[25] T. Nakamura, H. Shinohara, presented at *2007 IEEE Int. Conf. on Robotics and Automation*, Roma, Italy, April **2007**.

